SUPPLEMENTARY FIGURES

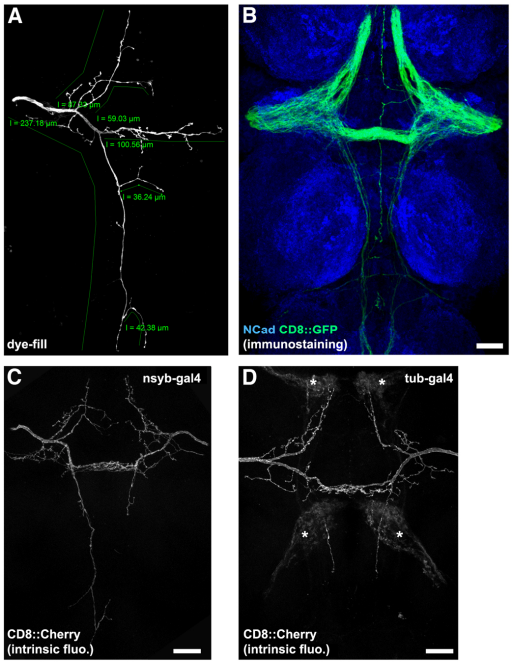

Figure S1. Labeling of single DC neurons.

(A) Dye-filled pDC neuron. Approximate length of individual branches is indicated. (B) Expression pattern of *pnr-gal4* in the VNC (driving UAS-mCD8::GFP as an axonal marker). Neuropil is counterstained with N-Cadherin (NCad). (C and D) DC1.4-Flp is sufficient for generating DC neuron specificity in the VNC. (C) VNC of a fly with the pan-neuronal driver *nsyb-gal4* in addition to *pnr-gal4*, in the *gal80* flp-out setup (see Table S1). A pDC neuron is labeled on the left, an aDC neuron on the right, and three microchaetae neurons are also labeled. (D) VNC of a fly with the ubiquitous driver *tub-gal4* in addition to *pnr-gal4*, in the *gal80* flp-out setup (see Table S1). On each side, a single aDC neuron is labeled. Asterisks indicate weak background signal in cellular processes that are located in a different optical plane. mCD8::mCherry expression in these processes likely arises due to incomplete suppression of the strong *tub-gal4* driver by *tub-gal80* (in the absence of a flp-out event). In both C and D, the labeling specificity is, as with *pnr-gal4* alone, restricted to DC neurons. Thus, DC1.4-Flp does not induce *gal80* flp-out in the lineage of any other neuron in the VNC (see also flp-out of the STOP cassette from the Brp BAC construct in Figs 6, S6, which corroborates this notion). Scale bars represent 20 µm.

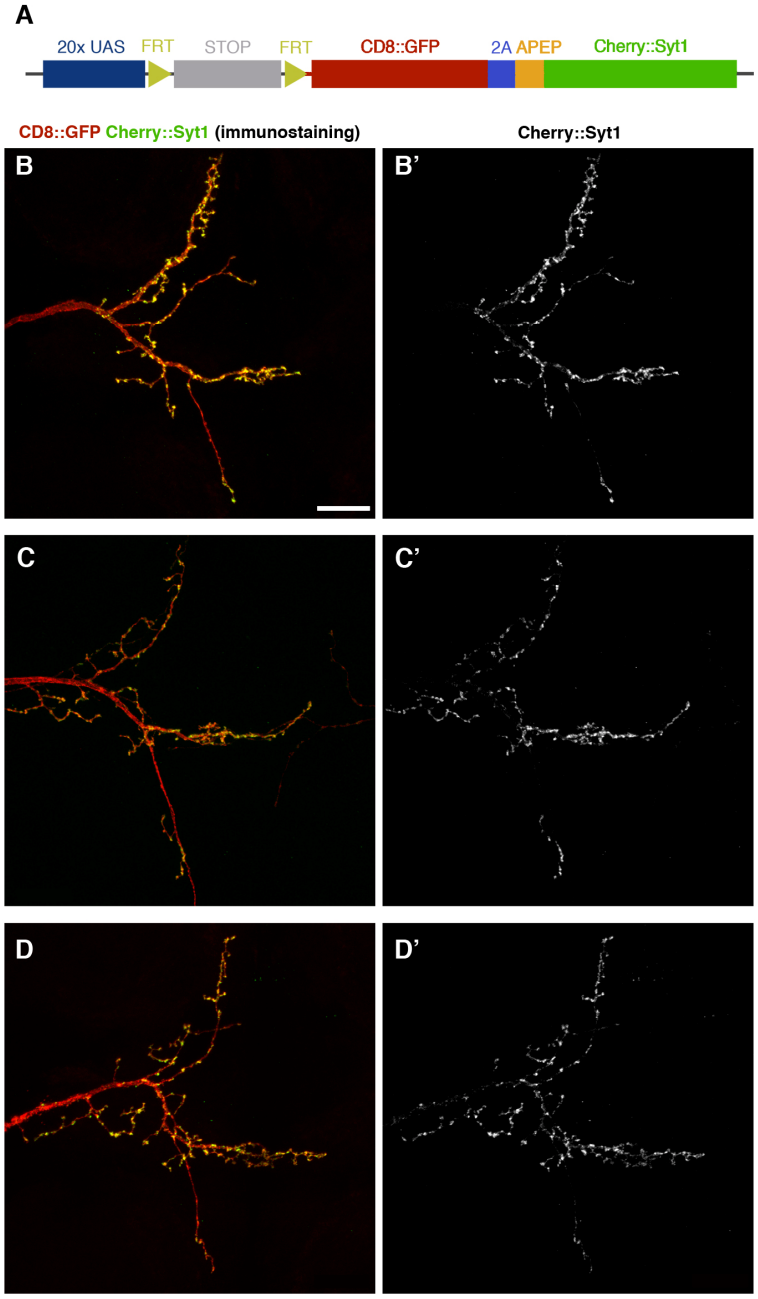

Figure S2. Structure and expression of 20xUAS-FRT>STOP>FRT-mCD8::GFP-2A-mCherry::Syt1. (A) Schematic illustrating the structure of the transgenic construct. "STOP": SV40 and α_1-tubulin transcriptional stop cassettes in tandem (Stockinger et al., 2005). FRT sites are the same as in (Potter et al., 2010). "2A" is the 2A peptide from the insect virus *Thosea asigna* (Szymczak et al., 2004). A ribosome skip at the 2A peptide ensures that mCD8::GFP and mCherry::Syt1 are produced as separate, individual proteins during translation (Donnelly et al., 2001). "APEP" is a consensus acceptor peptide for biotin ligase (Beckett et al., 1999), which was not used in this study. The different elements of the

construct are not drawn to scale. (B-D) Three different examples of single DC neurons labeled by DC1.4-Flp mediated excision of the STOP cassette in the above construct. For comparison, the neuron in panel B is the same as the one in Figure 2C. Note that a microchaeta-innervating neuron is also labeled on the right side in C. See also Fig. 7C, top panel, for a high-magnification heat-map of Cherry::Syt1 expressed from this construct. Scale bar is 20 μm.

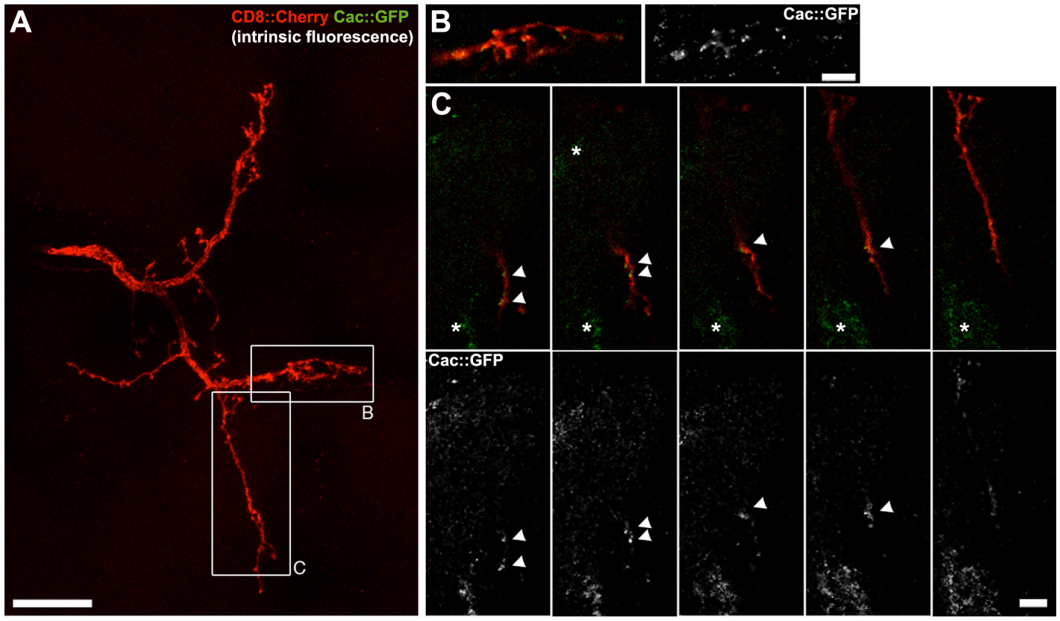

Figure S3. Cacophony::GFP expression in a single DC neuron.

(A) Single aDC neuron labeled using the *gal80* flp-out setup (see Fig. 1E), and expressing a GFP-tagged version of the pre-synaptic Calcium channel subunit Cacophony from a UAS construct (Kawasaki et al., 2004). Boxes indicate regions magnified in panels B-C. (B) Cac::GFP is observed in a punctate pattern in the midline region of the main commissure, similar to Brp^{short}::GFP (see Fig. 2M). (C) Like the other pre-synaptic markers and F-actin markers, Cac::GFP localizes specifically in a stereotypic location close to the tip of the posterior projection of the aDC neuron (arrowheads), and the more anterior region of this projection is devoid of marker. Consecutive single optical sections are shown, as specific Cac::GFP signal is weak in comparison to unspecific signal from other neurons (asterisks), and the latter appears more prominent in maximum intensity projections. Scale bars: 20 µm in A, 5 µm in B and C.

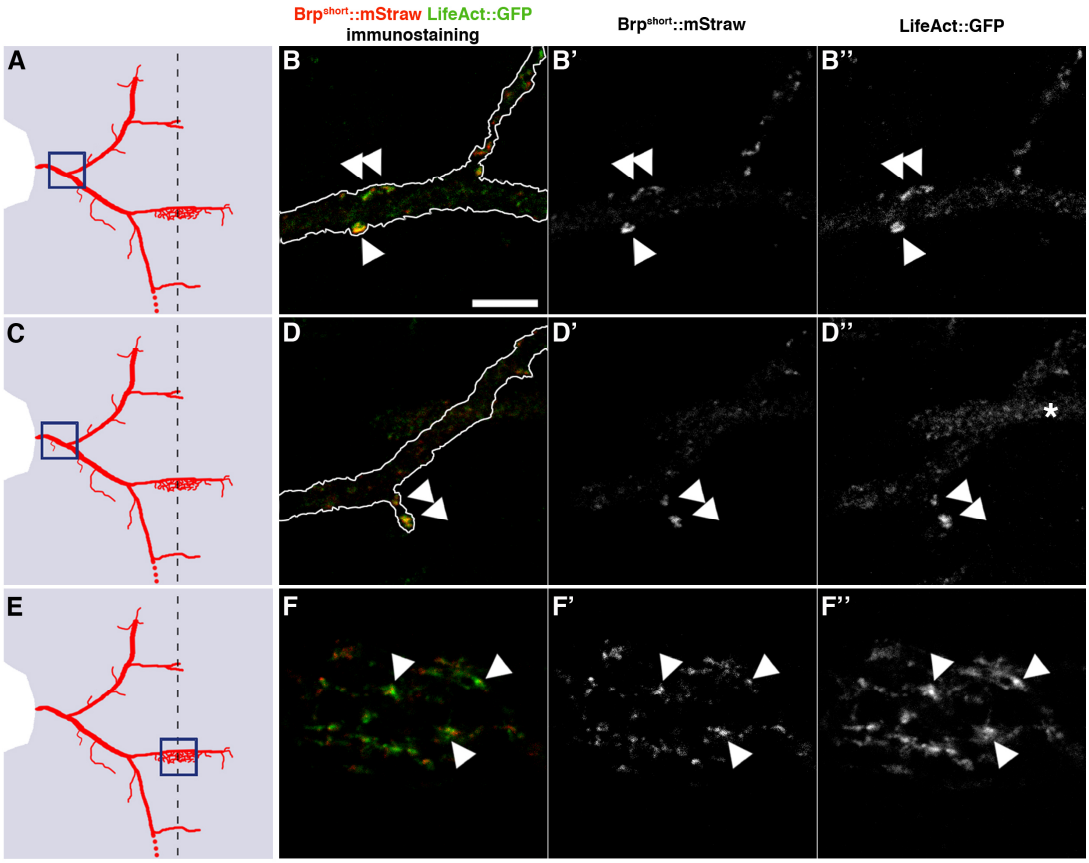

Figure S4. Co-localization of an active zone and a stable F-actin marker in DC neurons.

(A, C, E) Schematics illustrating the regions of the DC neurons (red) shown in B, D and F, respectively (blue boxes). (B) Co-localization of Brp^{short}::mStraw and LifeAct::GFP at *en passant* synapses (arrowheads) in the main axon proximal to the first branch point. (D) Co-localization of the two markers at terminal synapses of a small side branch (arrowheads; compare with side branch pointed out in Figure 3E). Asterisk in D'' indicates background fluorescence in another labeled neuron. (F) Co-localization of the markers at synapses (some of them pointed out by arrowheads) in the midline region of the main commissure. Outlines of axons (white lines) were traced in overexposed images (to reveal background fluorescence in the axons) and copied into panels B and D. B and F are single optical sections, D is a maximum projection of 3 optical sections. Scale bar represents 5 µm.

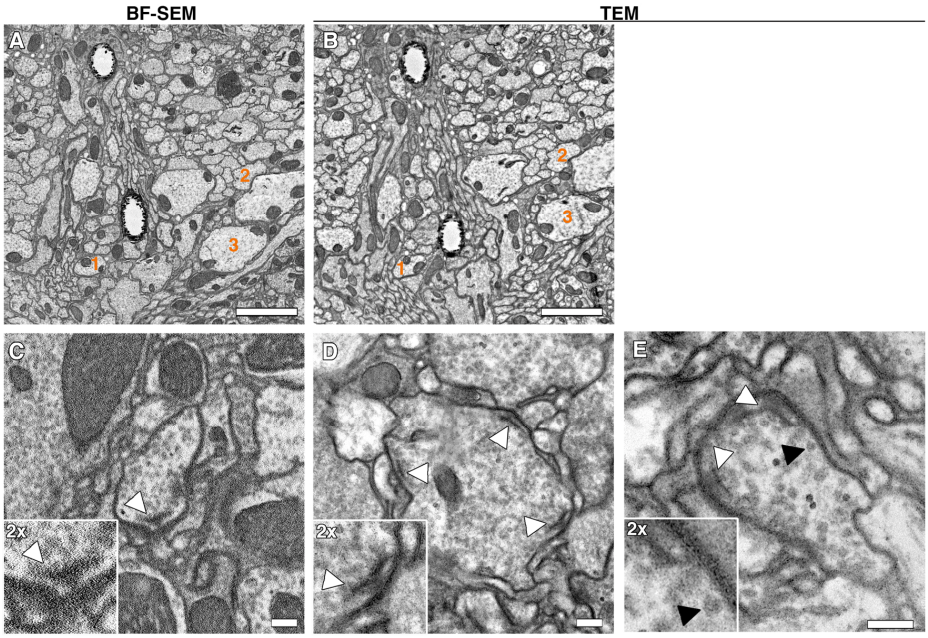

Figure S5. Comparison of EM imaging methods for synapses in the *Drosophila* adult VNC.

(A) Overview image of a VNC neuropil region imaged by BF-SEM. Sample was prepared with uranyl acetate and double osmication so as to generate enough contrast. (B) TEM image of a section taken from the block surface after BF-SEM imaging of the sample shown in A. Same neurites can be re-identified (some examples indicated by numbers). (C) High-magnification BF-SEM image of a synapse in the sample shown in A. Inset shows a 2x magnification of the T-bar-shaped active zone (arrowhead). (D) High-magnification TEM images of three synapses (active zones pointed out by arrowheads) in the same section as shown in B (same sample as in A and C). Note that lipid bilayers of plasma membranes can be seen in both the main panel and magnified inset. (E) TEM image of a section from another sample prepared with the high-contrast protocol for BF-SEM (same as for A-D). Pre-synaptic active zones are pointed out by white arrowheads. Note that the sample preparation protocol used for BF-SEM generates high contrast in membranes, but less for proteinaceous structures such as active zones. The latter are therefore less prominent than in samples prepared with a standard TEM protocol (see for example (Miskiewicz et al., 2014; Prokop and Meinertzhagen, 2006) for comparison), but are nevertheless clearly recognizable. Also note the visibility of the lipid bilayer in both the plasma membranes and synaptic vesicle membranes (latter pointed out by black arrowhead in both the main panel and inset of E). Scale bars: 2 µm in A and B, 200 nm in C-E.

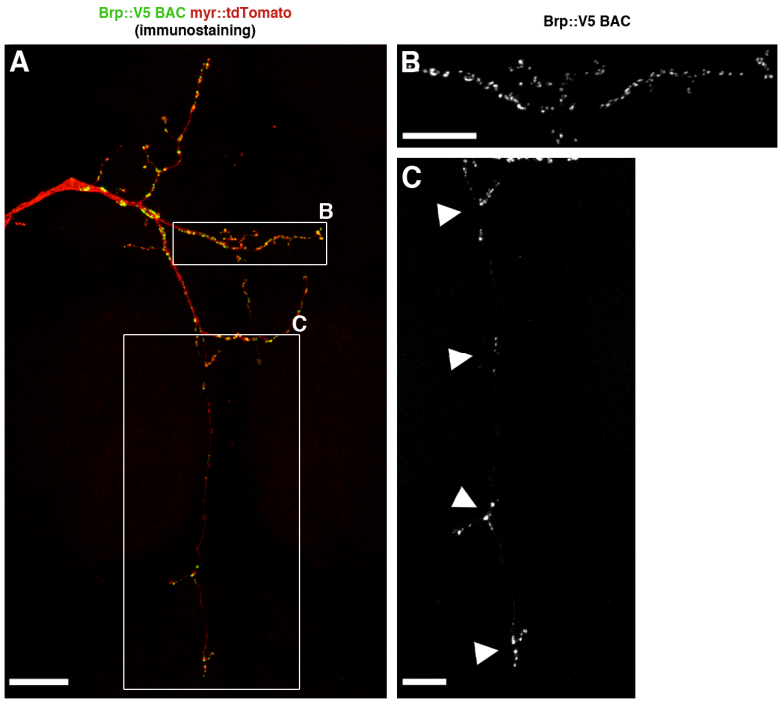

Figure S6. BAC-based expression of Brp::V5 in a pDC ms-neuron.

DC1.4-Flp was used to remove the FRT-flanked STOP cassette from the Brp BAC construct described in (Chen et al., 2014). (A) Co-labelling of Brp::V5 and myristoylated tdTomato to reveal pre-synaptic active zones and the whole pDC branch pattern. (B) Detail of the main commissure. Many active zones are located along the whole commissure and in the terminal synaptic branches in the midline region. (C) Detail of the posterior branch. Note that the Brp::V5 marker accumulates at precisely the same four stereotypic positions as Brp^{short}::GFP expressed from a UAS-construct (arrowheads point to the same locations as arrowheads in Figs. 2 B, D, E, 3 A-C). See Table S1 for full genotype. Scale bars: 20 µm in A, 10 µm in B and C.

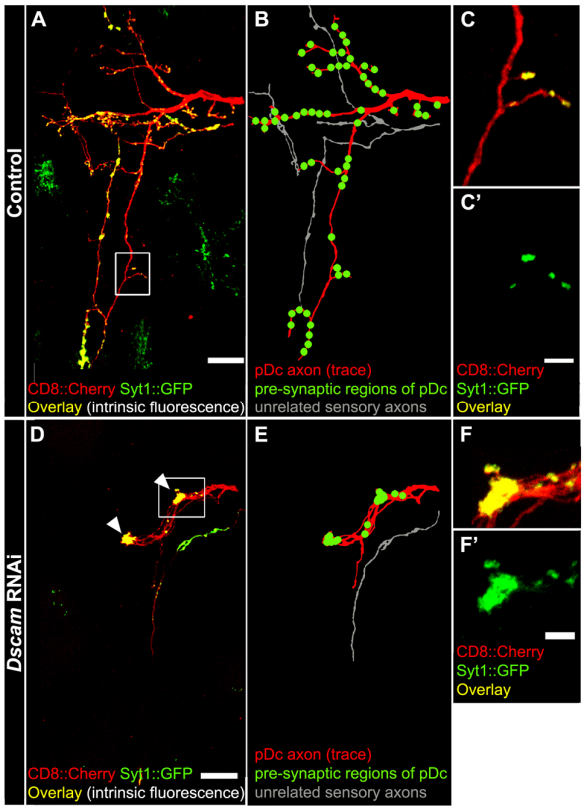

Figure S7. *Dscam* RNAi phenotype in the *gal80* flp-out setup.

(A) Control pDC neuron (labeling according to genotype in Figures 1E and Table S1). Unrelated neurons are also labeled (see panel B). (B) Manual tracing of the pDC neuron (red) and the axonal projections from unrelated neurons (grey), based on the image in A. Approximate locations of pre-synaptic marker are indicated by green circles. (C) Magnification of the region boxed in A, exemplifying appearance of terminal synapses labeled with Syt1::GFP. (D) Projection of a pDC neuron in an animal of the same genotype as in A, except that a UAS construct coding for a short hairpin targeting *Dscam* gene expression was crossed in. RNAi is induced only in the labeled neurons in this setup. Branches fail to segregate, and form clumps (arrowheads) instead of elaborating the normal arborization pattern. (E) Manual tracing of the axonal projections labeled in D. (F) Magnification of the region boxed in D. Syt1 pre-synaptic marker strongly accumulates in the clumps. See Table S2 for quantification of phenotypes. Scale bars: 20 µm in A and D, 5 µm in C and F.

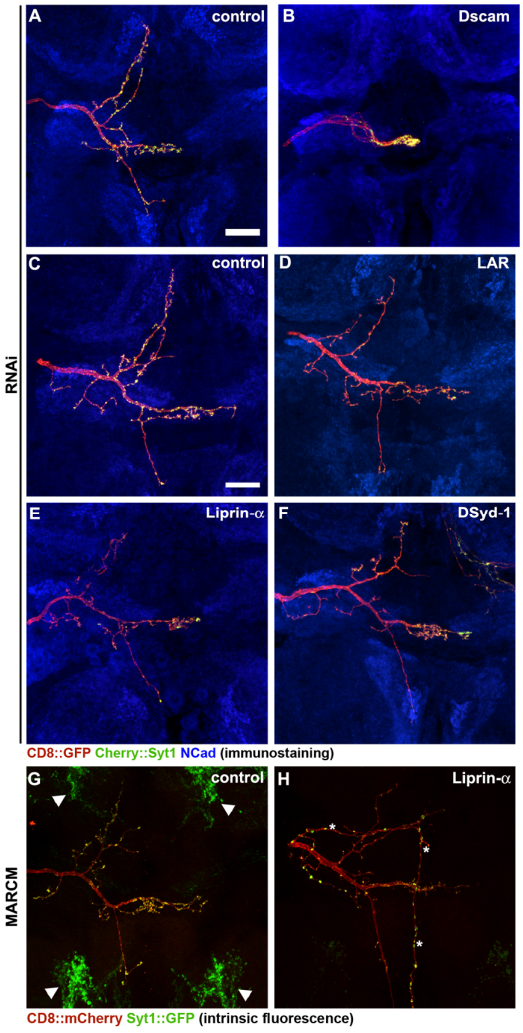

Figure S8. The axonal arborization pattern of DC neurons is defective upon knockdown of *Dscam*, but is normal upon loss-of-function of either *Lar*, *Liprin-α* or *DSyd-1*.

(A-F) The STOP cassette flp-out setup was used for labeling single DC neurons (see Fig. 1E' and Table S1, short hairpin RNAs are expressed in the whole *pnr* domain). (A) DC neuron arborization pattern in a control fly. (B) The branching pattern is completely abolished upon knockdown of *Dscam*, and all branches collapse into a clump, in this case on the midline, where high amounts of the Syt1 marker accumulate. See Table S2 for quantification of phenotypes. (C-F) Samples are the same as the ones shown in Fig. 7B,C. Neither RNAi targeting *Lar*, *Liprin-α* nor *DSyd-1* causes any axon branch targeting defects. Note that a few microchaetae neurons are also labeled on the right side of panel F. (G-H) MARCM according to the genotype shown in Table S1. Samples are the same as the ones shown in Fig. 7D. Note that for the Liprin-α sample, the maximum intensity projection in Fig. 7D shows a

subset of the confocal image stack (encompassing all midline processes), while in panel H of this figure, the maximum intensity projection of the whole stack is shown. In panel G, arrowheads point to unspecific signal arising from leakiness of the UAS-Syt1::GFP construct (the same is seen, but to a lesser extent, in panel H). In panel H, asterisks indicate the process of an unrelated neuron projecting along the midline. Scale bars, 20 µm.

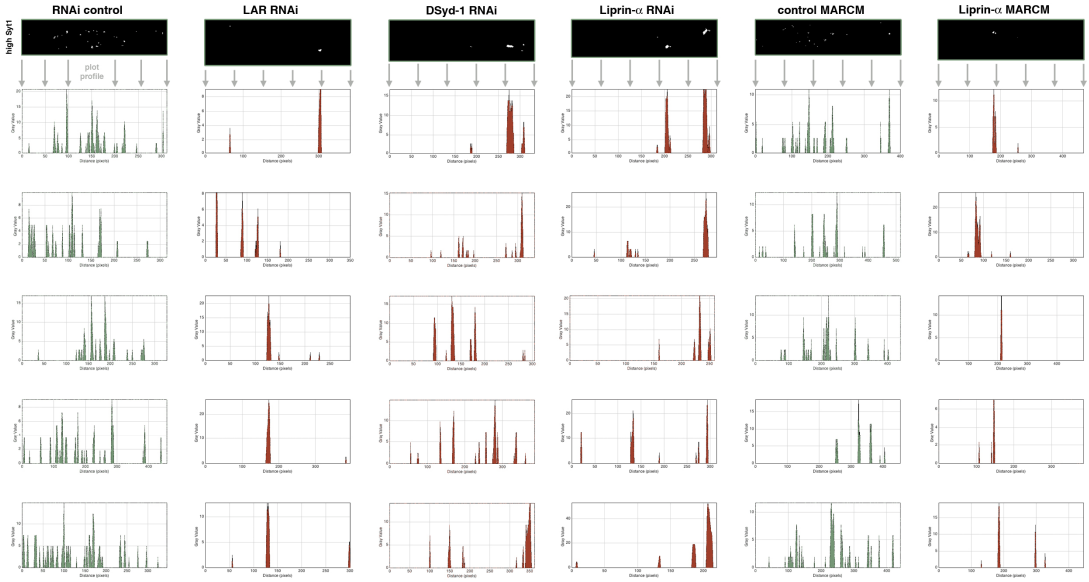

Figure S9. Graphical representation of Syt1 marker distribution in the main commissure of several control DC neurons and several *Lar*, *DSyd-1* and *Liprin-α* loss-of-function DC neurons.

Heat-maps of Syt1 signal (analogous to the ones shown in Fig. 7C and D) were transformed into binary images (top panels) so that pixels with very high Syt1 signal intensity (orange-red in heat-maps) appear white, and all other pixels appear black. Amounts of white pixels in each column of the binary image were then plotted along the midline as illustrated by gray arrows. Graphs of five representative samples of each genotype are shown. For comparison, top panels show binary images of the samples shown in Fig. 7, and graphs in the uppermost row correspond to these samples. Note that in controls, many peaks of strong Syt1 signal are distributed along the whole commissure, with a certain enrichment in the midline region (due to the high number of terminal branches in this region). In contrast, upon loss-of-function of either *Lar*, *DSyd-1* or *Liprin-α*, strong Syt1 signal often accumulates in only very few main peaks that can be located at different positions along the midline.

Immunostaining for Cherry::Syt1 was used in RNAi samples (columns 1-4), intrinsic fluorescence of Syt1::GFP was used in MARCM samples (columns 5 and 6).

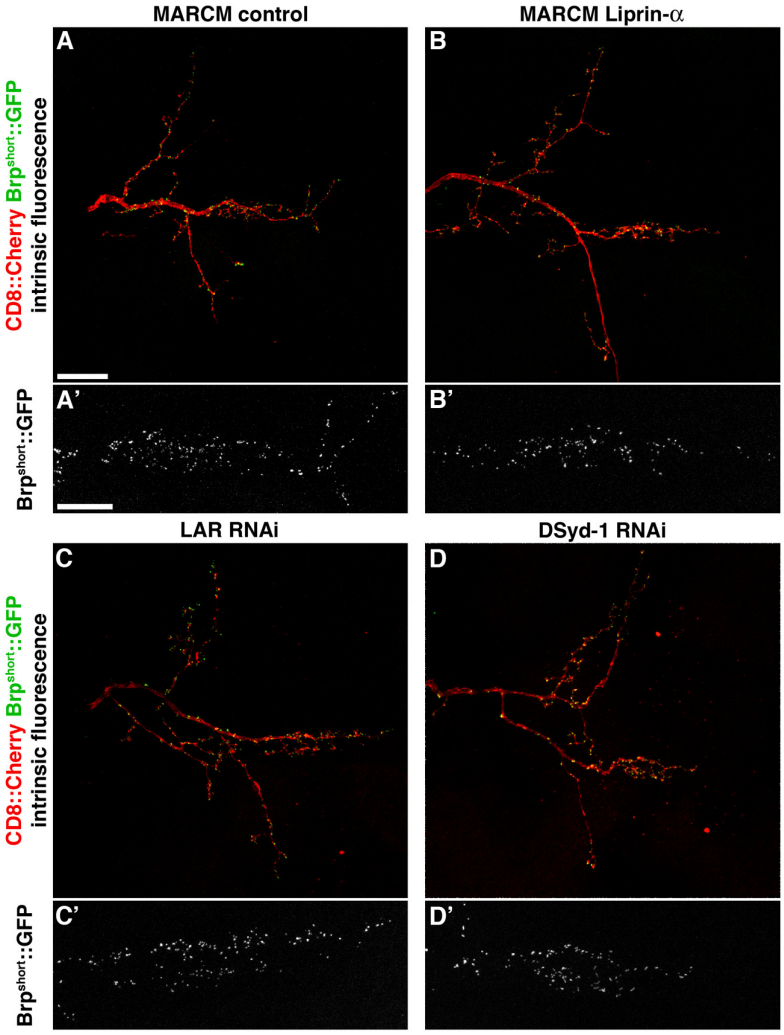

Figure S10. The active zone marker Brp^{short}::GFP accumulates normally in ms neurons depleted of *Liprin-α*, *Lar* or *DSyd-1*.

(A) Single DC neuron control MARCM clone. The whole arborization pattern and localization of Brp^{short}::GFP are shown in A. A' shows a detail of Brp^{short}::GFP localization on the main commissure (analogous in B/B', C/C' and D/D'). (B-D) No phenotypes in branching or Brp^{short}::GFP localization were observed for either Liprin-α mutant MARCM clones (n=7), Lar knockdown (n=13) or DSyd-1 knockdown (n=10). Scale bars represent 20 μm in A and 10 μm in A'.

Table S1. Genotypes of flies used in this study

Figure	Genotype
1B	*w; UAS-CD8::mCherry(ChRFP) / +; pnr-gal4 / +*
1C	*DC1.4-nGFP*
1D,H,I,L,M	*w; DC1.4-Flp / +; UAS-FRT>STOP>FRT-CD8::GFP-2A-APEP-mCherry::Syt1 pnr-gal4 / +*
1J,K	*w; FRTG13 tub-gal80 / FRTG13; pnr-gal4 UAS-CD8::Cherry UAS-Syt1::GFP / DC1.4-Flp*
2B,K-O	*w tub>gal80> / +; UAS-Brp^{short}::GFP DC1.4-Flp / +; pnr-gal4 UAS-CD8::mCherry / +*
2C,D	*w; DC1.4-Flp / +; UAS-FRT>STOP>FRT-CD8::GFP-2A-APEP-mCherry::Syt1 pnr-gal4 / +*
2G-I	*w tub>gal80> / +; DC1.4-Flp / UAS-Brp^{short}::mStraw; UAS-Syt1::GFP / pnr-gal4*
3A	*w tub>gal80> / +; UAS-UtABD::GFP DC1.4-Flp / +; pnr-gal4 UAS-CD8::mCherry / +*
3B,E,F	*w tub>gal80> / +; UAS-LifeAct::GFP DC1.4-Flp / +; pnr-gal4 UAS-CD8::mCherry / +*
3C,G,H	*w tub>gal80> / +; DC1.4-Flp / UAS-GFP::Actin; pnr-gal4 UAS-CD8::mCherry / +*
3I	*w tub>gal80> / +; DC1.4-Flp / +; pnr-gal4 UAS-CD8::mCherry / UAS-GFP::□1-tub84B*
3J-L	*w tub>gal80> / +; DC1.4-Flp / UAS-mito-HA::GFP; pnr-gal4 UAS-CD8::mCherry / +*
4	*w tub>gal80> / +; UAS-Brp^{short}::GFP DC1.4-Flp / +; pnr-gal4 UAS-CD8::mCherry / +*
5B-M	*w tub>gal80> / +; UAS-Brp^{short}::GFP DC1.4-Flp / +; pnr-gal4 UAS-CD8::mCherry / +*
5O	*w tub>gal80>; DC1.4-Flp / UAS-mito-HA::GFP; pnr-gal4 UAS-CD8::mCherry / +*
5P,Q	*w tub>gal80> / +; UAS-Brp^{short}::GFP DC1.4-Flp / +; pnr-gal4 UAS-CD8::mCherry / +*
6A	*w tub>gal80> / +; UAS-Brp^{short}::GFP DC1.4-Flp / +; pnr-gal4 UAS-CD8::mCherry / +*
6B	*w; LexAop-myr-tdTomato PBac{brp-FRT>STOP>FRT-V5-2A-LexAVP16} / +; DC1.4-Flp / +*
7B,C control	*w / y w; DC1.4-Flp / P{attP,y[+],w[3`]}; UAS-FRT>STOP>FRT-CD8::GFP-2A-APEP-mCherry::Syt1 pnr-gal4 / +*
Lar	*w / y v; DC1.4-Flp / P{TRiP.HMS02186}; UAS-FRT>STOP>FRT-CD8::GFP-2A-APEP-mCherry::Syt1 pnr-gal4 / +*
Liprin-α	*w / y w; DC1.4-Flp / UAS-IR^{KK106588}; UAS-FRT>STOP>FRT-CD8::GFP-2A-APEP-mCherry::Syt1 pnr-gal4 / +*
DSyd-1	*w / y w; DC1.4-Flp / UAS-IR^{KK106241}; UAS-FRT>STOP>FRT-CD8::GFP-2A-APEP-mCherry::Syt1 pnr-gal4 / +*
7D control	*w; tub-gal80 FRT40A / P{□M}36F FRT40A; pnr-gal4 UAS-Syt1::GFP UAS-CD8::mCherry / DC1.4-Flp*
Liprin-α	*w; tub-gal80 FRT40A / Liprin-α^{DG23609} FRT40A; pnr-gal4 UAS-Syt1::GFP UAS-CD8::mCherry / DC1.4-Flp*
S1B	*w; UAS-CD8::GFP / +; pnr-gal4 / +*

S1C	*w tub>gal80> / +; DC1.4-Flp / +; pnr-gal4 UAS-CD8::mCherry / nsyb-gal4*
S1D	*w tub>gal80> / +; DC1.4-Flp / +; pnr-gal4 UAS-CD8::mCherry / tub-gal4*
S2	*w / (y) w or Y; DC1.4-Flp / +; UAS-FRT>STOP>FRT-CD8::GFP-2A-APEP-mCherry::Syt1 pnr-gal4 / + ((y) w background)*
S3	*w tub>gal80> / +; DC1.4-Flp / UAS-CD8::Cherry; pnr-gal4 / UAS-Cac::GFP*
S4	*w tub>gal80> / +; DC1.4-Flp UAS-LifeAct::GFP / UAS-Brp^{short}::mStraw; pnr-gal4 / +*
S6	*w; LexAop-myr-tdTomato PBac{brp-FRT>STOP>FRT-V5-2A-LexAVP16}/ +; DC1.4-Flp / +*
S7A,C	*w tub>gal80> / w; DC1.4-Flp / +; pnr-gal4 UAS-Syt1::GFP UAS-CD8::Cherry / +*
S7D,F	*w tub>gal80> / y w; DC1.4-Flp / UAS-IR^{KK108835}; pnr-gal4 UAS-Syt1::GFP UAS-CD8::Cherry / +*
S8A	*w / +; DC1.4-Flp / +; UAS-FRT>STOP>FRT-CD8::GFP-2A-APEP-mCherry::Syt1 pnr-gal4 / + (CantonS background)*
S8B	*w / y w; DC1.4-Flp / UAS-IR^{KK108835}; UAS-FRT>STOP>FRT-CD8::GFP-2A-APEP-mCherry::Syt1 pnr-gal4 / +*
S8C	*w / y w; DC1.4-Flp / P{attP,y[+],w[3`]}; UAS-FRT>STOP>FRT-CD8::GFP-2A-APEP-mCherry::Syt1 pnr-gal4 / +*
S8D	*w / y v; DC1.4-Flp / P{TRiP.HMS02186}; UAS-FRT>STOP>FRT-CD8::GFP-2A-APEP-mCherry::Syt1 pnr-gal4 / +*
S8E	*w / y w; DC1.4-Flp / UAS-IR^{KK106588}; UAS-FRT>STOP>FRT-CD8::GFP-2A-APEP-mCherry::Syt1 pnr-gal4 / +*
S8F	*w / y w; DC1.4-Flp / UAS-IR^{KK106241}; UAS-FRT>STOP>FRT-CD8::GFP-2A-APEP-mCherry::Syt1 pnr-gal4 / +*
S8G	*w; tub-gal80 FRT40A / P{▫M}36F FRT40A; pnr-gal4 UAS-Syt1::GFP UAS-CD8::mCherry / DC1.4-Flp*
S8H	*w; tub-gal80 FRT40A / Liprin-α^{DG23609} FRT40A; pnr-gal4 UAS-Syt1::GFP UAS-CD8::mCherry / DC1.4-Flp*
S10A	*w; tub-gal80 FRT40A / P{▫M}36F FRT40A; pnr-gal4 DC1.4-Flp / UAS- brp^{short}::GFP UAS-CD8::Cherry*
S10B	*w; tub-gal80 FRT40A / Liprin-▫^{DG23609} FRT40A; pnr-gal4 DC1.4-Flp / UAS- brp^{short}::GFP UAS-CD8::Cherry*
S10C	*w tub>gal80> / +; DC1.4-Flp UAS-brp^{short}::GFP / P{TRiP.HMS02186}^{attP40}; pnr-gal4 UAS-CD8::Cherry / +*
S10D	*w tub>gal80> / +; DC1.4-Flp UAS-brp^{short}::GFP / UAS-IR^{KK106241}; pnr-gal4 UAS-CD8::Cherry / +*

Table S2. Quantification of *Dscam* RNAi knockdown phenotypes.

			% displaying given phenotype				
Genetic setup[a]	Genotype	Temperature	normal	1 defective[b]	2 defective[b]	all 3 defective[b]	n[c]
gal80 flp-out	control	25°C	100	0	0	0	11
gal80 flp-out	*Dscam* RNAi	25°C	26	45	16	13	33
gal80 flp-out	control	29°C	100	0	0	0	9
gal80 flp-out	*Dscam* RNAi	29°C	15	31	23	31	13
STOP flp-out	control	25°C	100	0	0	0	12
STOP flp-out	*Dscam* RNAi	25°C	0	0	25	75	4

[a]: "gal80 flp-out" corresponds to the setup shown in Fig. 1E, "STOP flp-out" to the one in Fig. 1E'.

[b]: The three main primary branches (projecting towards anterior, posterior, and crossing the midline, respectively) were scored. For the anterior and posterior projecting branches, their absence was scored as "defective". The midline crossing branch was scored as defective when it did not extend beyond the midline but instead stalled there. For example, the neuron shown in Fig. S7E was scored as "2 defective": the anterior branch is absent, and the midline-crossing branch does not project beyond the midline. "All 3 defective" designates neurons where all branches collapse into a single clump (see for example Fig. S8B).

[c]: "n" indicates numbers of neurons scored

SUPPLEMENTARY MATERIALS AND METHODS

Molecular biology and constructs

For DC1.4-Flp construction, Flp coding sequence amplified from pUAST-FLP (Duffy et al., 1998) was inserted into a pHStinger plasmid containing the ~1.4 kb DC enhancer ("DCE", (Marcellini and Simpson, 2006)) by using *PmeI* / *HpaI*, thus replacing the GFP coding sequence in the plasmid by Flp coding sequence.

Construction of 20xUAS-FRT>STOP>FRT-mCD8::GFP-2A-mCherry::Syt1 (Fig. S2):

mCD8::GFP was amplified with the primer pair 5'-ATAAGAATGCGGCCGCCACCATGGCCTCACCGTTGACCCG-3' / 5'-CTCGTGCCACTCGATCTTCTGGGCCTCGAAGATGTCGTTCAGGCCCGGGCCCGGGTTCTCC TCGACGTCGCCGCAGGTCAGCAGGCTGCCCCTGCCCTCGCCGCTGCCTTTGTATAGTTCAT CCATGCCATG-3'. mCherry was amplified with the primers 5'-GGCCCAGAAGATCGAGTGGCACGAGATGGTGAGCAAGGGCGAGGA-3' / 5'-TGCTCTAGATTACTTGTACAGCTCGTCCATGC-3'. The primers contain the sequence of the 2A peptide from *Thosea asigna*, which induces a ribosome skip during translation (Szymczak et al., 2004), and a sequence encoding a consensus acceptor peptide for biotin ligase (Beckett et al., 1999), which was not used in this study. The two PCR products were fused by overlap PCR and inserted into a cloning vector. Subsequently, 9 bp (GGCAGCGGC) encoding a GSG spacer were introduced between the acceptor peptide and mCherry, and the STOP codon of mCherry was removed by mutagenesis. To amplify the Syt1 coding region (CDS), genomic DNA was extracted from UAS-Syt1::GFP flies (Zhang et al., 2002), and Syt1 CDS was amplified using the primer pair 5'-AACTAGCTAGCGGTATGCCGCCAAATGCAAAATCG-3' / 5'-GCTCTAGATTACTTCATGTTCTTCAGGATCTCG-3'. The Syt1 PCR product was digested with NheI and XbaI enzymes (New England Biolabs), and inserted into the vector containing mCD8::GFP-2A-mCherry, which had been cut with XbaI and de-phosphorylated by shrimp alkaline phosphatase (Fermentas). Clones with the right insert directionality were selected by restriction digest with NdeI. Subsequently, a NotI / XbaI fragment of this plasmid was subcloned into NotI / XbaI-digested pJFRC7 (Pfeiffer et al., 2010), replacing mCD8::GFP of pJFRC7 by mCD8::GFP-2A-mCherry::Syt1. Finally, FRT>STOP>FRT was excised from pUAS-FRT>STOP>FRT-mCD8::GFP (Potter et al., 2010) using

BglII, and cloned into the BglII site of pJFRC7-mCD8::GFP-2A-mCherry::Syt1 to generate pJFRC7-20xUAS-FRT>STOP>FRT-mCD8::GFP-2A-mCherry::Syt1. Clones of right insert directionality were identified by colony PCR and verified by restriction digest with ClaI. All PCR products were generated by KOD proofreading polymerase (Merck Millipore), and the intermediate and final plasmids were verified by sequencing.

Drosophila genetics, stocks and _in vivo_ RNAi

Flies were reared on standard fruit fly medium at 25°C or 29°C. Transgenic flies were generated using standard P-element (DC1.4-Flp) or PhiC31-mediated transformation (20xUAS-FRT>STOP>FRT-mCD8::GFP-2A-mCherry::Syt1, integrated into landing platform attP2 (Groth et al., 2004)), at Genetic Services or Rainbow Transgenic Flies, respectively.

Fly stocks used are: CantonS, w^{1118}, and y w as control backgrounds. ptub > gal80 > (Gordon and Scott, 2009); pnr-gal4 (Calleja et al., 1996); nsyb-gal4 (Hugo Bellen, personal communication to FlyBase); tub-gal4 (Lee and Luo, 1999); UAS-mCD8::GFP (Lee and Luo, 1999); UAS-mCD8::ChRFP (UAS-mCD8::mCherryRFP, Frank Schnorrer, personal communication to FlyBase); UAS-Syt1::GFP (Zhang et al., 2002); UAS-Brp^{short}::GFP (Fouquet et al., 2009); UAS-Brp^{short}::mStraw (Owald et al., 2010); P{LexAop-tdTomato.Myr}^{attP5} PBac{brp(FRT.Stop)V5-2A-LexA-VP16}^{VK00018}/CyO (Chen et al., 2014); TM2/TM6B, Tb1 UAS-mito-GFP (Aaron Pilling and Bill Saxton, personal communication to FlyBase); UAS-GFP-α1-tub84B (Grieder et al., 2000); UAS-LifeAct::GFP (Hatan et al., 2011); UAS-Utr::GFP (Rauzi et al., 2010); UAS-GFP::Actin (Verkhusha et al., 1999); UAS-Cac::GFP (Kawasaki et al., 2004); UAS-Dscam-hairpin RNA (hpRNA, Vienna *Drosophila* RNAi Center, VDRC, line KK 108835); UAS-Liprin-α-hpRNA (VDRC, line KK 106588); UAS-DSyd-1-hpRNA (VDRC, line KK 106241); UAS-Lar-short hairpin RNA (Transgenic RNAi Project at Harvard Medical School, line HMS02186); y,w^{1118}; P{attP,y^{+},$w^{3`}$} (VDRC, transformant ID 60100, control line for RNAi experiments); w^{*}; P{FRT(w^{hs})}G13 (Norbert Perrimon, personal communication to FlyBase); w^{1118}; P{αM}36F P{neoFRT}40A (Xu and Rubin, 1993); P{y^{+} w^{+mC}=wHy}Liprin-α^{DG23609} P{ry^{+}=neoFRT}40A (Chen et al., 2005).

To assess strength of RNAi-induced knockdown of gene expression in ms-neurons, we compared the two genetic setups shown in Fig. 1E,E', in combination with *Dscam* RNAi. In the first case (Fig. 1E), *gal80* excision induces RNAi only in the labeled neurons. However, Gal80 perdurance is expected to

delay RNAi during ms-neuron development, and thus to potentially lead to weak phenotypes. This setup allows screening for genes that have a strictly cell-intrinsic function in ms-neurons. In the second case (Fig. 1E') RNAi is induced in the whole *pnr-gal4* domain, independently of single neuron labeling. While knockdown may be earlier and / or stronger in this situation, genes causing phenotypes by non-cell autonomous mechanisms may also be recovered. A lower penetrance and expressivity was observed using the *gal80* flp-out system than the setup where the RNAi is expressed in the whole *pnr-gal4* pattern (Table S2).

Immunohistochemistry and light microscopy

For immunostainings, VNCs were dissected in 1x PBS and transferred to 2% paraformaldehyde (Electron Microscopy Sciences, EMS) in 1x PBS containing 0.1% Triton-X100 for a 1.5 hours-fixation at room temperature. Samples were rinsed and washed 4x >15 minutes in PBS-TX100, then blocked overnight at 4°C in 5% non-fat dry milk (Bio-Rad) in PBS-TX100 ("block solution"). The VNCs were then incubated 2 hours at room temperature in primary antibodies in block solution, rinsed 3x and washed 4x around 30 minutes at room temperature in PBS-TX100, then incubated 2 hours at room temperature in secondary antibodies in block solution, and rinsed and washed as above. Antibody incubations were increased to overnight at 4°C + 2 hours at room temperature for the co-staining experiments shown in Figs 2G-I and S4 to increase signal from Brp^{short}::mStraw, which is generally faint. Antibodies used were monoclonal nc82 and monoclonal DN-Ex #8 (both from the Developmental Studies Hybridoma Bank at the University of Iowa), monoclonal anti-GFP (9F9.F9, abcam), monoclonal anti-V5 (R960-25, Invitrogen), polyclonal anti-GFP (Invitrogen, #11122) and polyclonal anti-DsRed (Living Colors, Clontech). Carbocyanine dye labeling was performed as described previously (Chen et al., 2006). For imaging native GFP and mCherry fluorescence, VNCs were fixed for 1.5 hours at room temperature in 2% paraformaldehyde (EMS) in PBS-TX100, and then rinsed and washed around 2 hours in PBS-TX100. Except dye-labeled samples, which were imaged in carbonate buffer, all samples were mounted in Vectashield (Vector Laboratories) prior to imaging with a Zeiss LSM710 confocal microscope with a 40X/1.2 water immersion or a 100X/1.4 oil immersion objective.

Image processing, segmentation and 3D reconstruction

Contrast and brightness of fluorescence microscopy images were adjusted in the ZEN software (Zeiss), Fiji / ImageJ (Schindelin et al., 2012) and / or Adobe Photoshop, applying changes to whole images only. For comparison of Syt1 signal and generation of heat-maps (Figs 7, S9), contrast and brightness of the Syt1 channel were first adjusted in the ZEN software such that the images of the different experimental conditions have comparable background threshold, and saturation. This ensures that relative (but not absolute) amounts of fluorescence signals at different positions along the commissure can be compared inbetween samples. The images were then loaded into Fiji, where heat-maps were made using the HeatMap Histogram plugin.

Imod (http://bio3d.colorado.edu/imod/) and Fiji / ImageJ were used for registration of the 3D EM image stacks and converting to tif file-format. Segmentation of ms-axons and mitochondria from these datasets was performed either using the seeded watershed algorithm of the ilastik software (Sommer et al., 2011) or manually in the Fiji plugin TrakEM2 (Cardona et al., 2012). Contrast enhancement and pseudo-coloring of EM images was done in Adobe Photoshop.

Transmission electron microscopy

For imaging by TEM, the resin-embedded samples mounted on a pin and imaged previously by BF-SEM were clamped into the chuck of a Leica UCT ultramicrotome, 50 – 70 nm sections were cut and imaged in a JEOL JEM1400 transmission electron microscope at 80kV.

SUPPLEMENTARY REFERENCES

Beckett, D., Kovaleva, E. and Schatz, P. J. (1999). A minimal peptide substrate in biotin holoenzyme synthetase-catalyzed biotinylation. *Protein Sci* **8**, 921–929.

Calleja, M., Moreno, E., Pelaz, S. and Morata, G. (1996). Visualization of gene expression in living adult Drosophila. *Science* **274**, 252–255.

Cardona, A., Saalfeld, S., Schindelin, J., Arganda-Carreras, I., Preibisch, S., Longair, M., Tomancak, P., Hartenstein, V. and Douglas, R. J. (2012). TrakEM2 software for neural circuit reconstruction. *PLoS ONE* **7**, e38011.

Chen, B. E., Kondo, M., Garnier, A., Watson, F. L., Püettmann-Holgado, R., Lamar, D. R. and Schmucker, D. (2006). The molecular diversity of Dscam is functionally required for neuronal wiring specificity in Drosophila. *Cell* **125**, 607–620.

Chen, J., Call, G. B., Beyer, E., Bui, C., Cespedes, A., Chan, A., Chan, J., Chan, S., Chhabra, A., Dang, P., et al. (2005). Discovery-based science education: functional genomic dissection in Drosophila by undergraduate researchers. *PLoS Biol* **3**, e59.

Chen, Y., Akin, O., Nern, A., Tsui, C. Y. K., Pecot, M. Y. and Zipursky, S. L. (2014). Cell-type-Specific Labeling of Synapses In Vivo through Synaptic Tagging with Recombination. *Neuron* **81**, 280–293.

Donnelly, M. L., Luke, G., Mehrotra, A., Li, X., Hughes, L. E., Gani, D. and Ryan, M. D. (2001). Analysis of the aphthovirus 2A/2B polyprotein 'cleavage' mechanism indicates not a proteolytic reaction, but a novel translational effect: a putative ribosomal "skip." *J Gen Virol* **82**, 1013–1025.

Duffy, J. B., Harrison, D. A. and Perrimon, N. (1998). Identifying loci required for follicular patterning using directed mosaics. *Development* **125**, 2263–2271.

Fouquet, W., Owald, D., Wichmann, C., Mertel, S., Depner, H., Dyba, M., Hallermann, S., Kittel, R. J., Eimer, S. and Sigrist, S. J. (2009). Maturation of active zone assembly by Drosophila Bruchpilot. *J Cell Biol* **186**, 129–145.

Gordon, M. D. and Scott, K. (2009). Motor Control in a Drosophila Taste Circuit. *Neuron* **61**, 373–384.

Grieder, N. C., de Cuevas, M. and Spradling, A. C. (2000). The fusome organizes the microtubule network during oocyte differentiation in Drosophila. *Development* **127**, 4253–4264.

Groth, A. C., Fish, M., Nusse, R. and Calos, M. P. (2004). Construction of transgenic Drosophila by using the site-specific integrase from phage phiC31. *Genetics* **166**, 1775–1782.

Hatan, M., Shinder, V., Israeli, D., Schnorrer, F. and Volk, T. (2011). The Drosophila blood brain barrier is maintained by GPCR-dependent dynamic actin structures. *J Cell Biol* **192**, 307–319.

Kawasaki, F., Zou, B., Xu, X. and Ordway, R. W. (2004). Active zone localization of presynaptic calcium channels encoded by the cacophony locus of Drosophila. *J Neurosci* **24**, 282–285.

Lee, T. and Luo, L. (1999). Mosaic analysis with a repressible cell marker for studies of gene function in neuronal morphogenesis. *Neuron* **22**, 451–461.

Marcellini, S. and Simpson, P. (2006). Two or four bristles: functional evolution of an enhancer of scute in Drosophilidae. *PLoS Biol* **4**, e386.

Miskiewicz, K., Jose, L. E., Yeshaw, W. M., Valadas, J. S., Swerts, J., Munck, S., Feiguin, F., Dermaut, B. and Verstreken, P. (2014). HDAC6 Is a Bruchpilot Deacetylase that Facilitates Neurotransmitter Release. *Cell Rep.*

Owald, D., Fouquet, W., Schmidt, M., Wichmann, C., Mertel, S., Depner, H., Christiansen, F., Zube, C., Quentin, C., Körner, J., et al. (2010). A Syd-1 homologue regulates pre- and postsynaptic maturation in Drosophila. *J Cell Biol* **188**, 565–579.

Pfeiffer, B. D., Ngo, T.-T. B., Hibbard, K. L., Murphy, C., Jenett, A., Truman, J. W. and Rubin, G. M. (2010). Refinement of tools for targeted gene expression in Drosophila. *Genetics* **186**, 735–755.

Potter, C. J., Tasic, B., Russler, E. V., Liang, L. and Luo, L. (2010). The Q System: A Repressible Binary System for Transgene Expression, Lineage Tracing, and Mosaic Analysis. *Cell* **141**, 536–548.

Prokop, A. and Meinertzhagen, I. A. (2006). Development and structure of synaptic contacts in Drosophila. *Semin Cell Dev Biol* **17**, 20–30.

Rauzi, M., Lenne, P.-F. and Lecuit, T. (2010). Planar polarized actomyosin contractile flows control epithelial junction remodelling. *Nature* **468**, 1110–1114.

Schindelin, J., Arganda-Carreras, I., Frise, E., Kaynig, V., Longair, M., Pietzsch, T., Preibisch, S., Rueden, C., Saalfeld, S., Schmid, B., et al. (2012). Fiji: an open-source platform for biological-image analysis. *Nat Meth* **9**, 676–682.

Sommer, C., Straehle, C., Kothe, U. and Hamprecht, F. A. (2011). Ilastik: Interactive learning and segmentation toolkit.pp. 230–233. IEEE.

Stockinger, P., Kvitsiani, D., Rotkopf, S., Tirián, L. and Dickson, B. J. (2005). Neural circuitry that governs Drosophila male courtship behavior. *Cell* **121**, 795–807.

Szymczak, A. L., Workman, C. J., Wang, Y., Vignali, K. M., Dilioglou, S., Vanin, E. F. and Vignali, D. A. A. (2004). Correction of multi-gene deficiency in vivo using a single "self-cleaving" 2A peptide-based retroviral vector. *Nat Biotechnol* **22**, 589–594.

Verkhusha, V. V., Tsukita, S. and Oda, H. (1999). Actin dynamics in lamellipodia of migrating border cells in the Drosophila ovary revealed by a GFP-actin fusion protein. *FEBS Lett* **445**, 395–401.

Xu, T. and Rubin, G. M. (1993). Analysis of genetic mosaics in developing and adult Drosophila tissues. *Development* **117**, 1223–1237.

Zhang, Y. Q., Rodesch, C. K. and Broadie, K. (2002). Living synaptic vesicle marker: synaptotagmin-GFP. *Genesis* **34**, 142–145.